iScience

CellPress
OPEN ACCESS

Article

Cannabidiol counters the effects of a dominant-negative pathogenic Kv7.2 variant

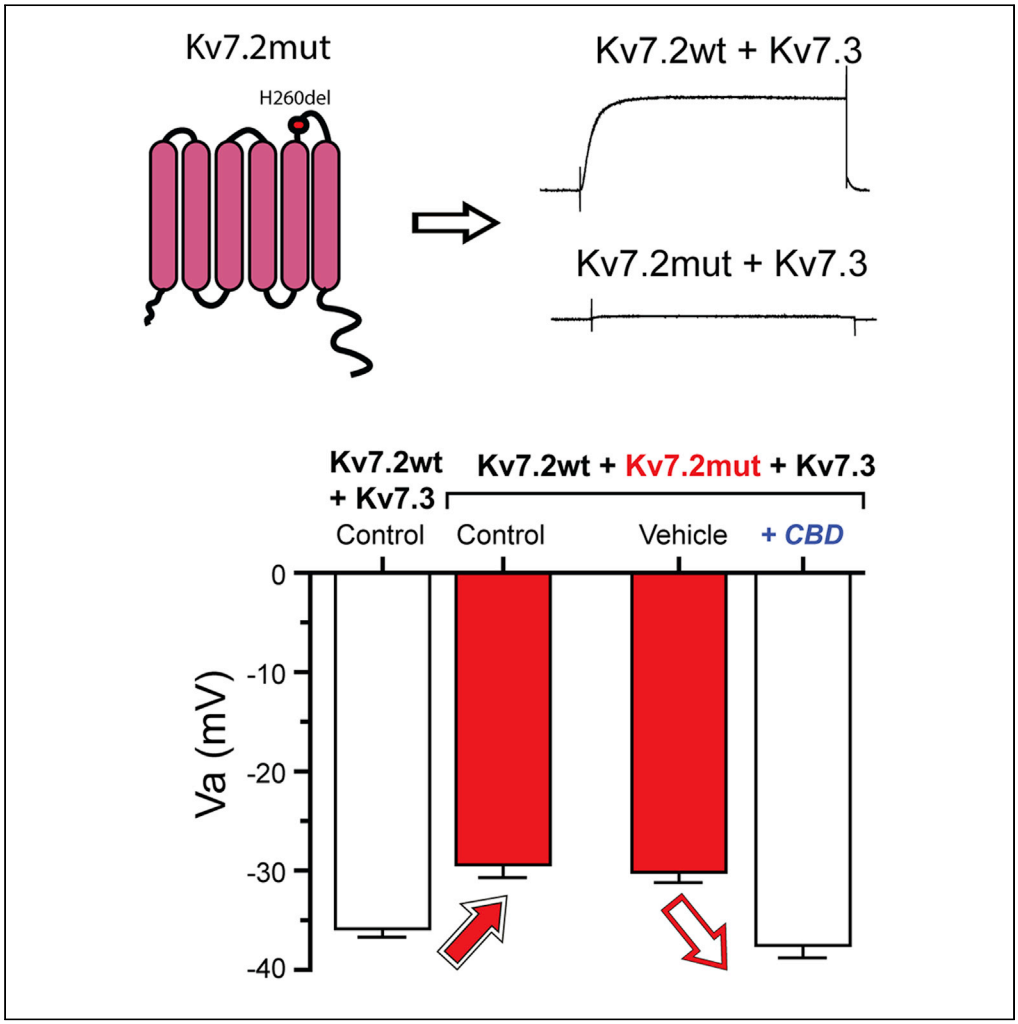

Xiaoqin Zhan, Chris Drummond-Main, Dylan Greening, ..., J.P. Appendino, P. Y. Billie Au, Ray W. Turner

rwturner@ucalgary.ca

Highlights

A patient with epileptic encephalopathy exhibits a Kv7.2 deletion at H260 (Kv7.2mut)

Kv7.2mut shows increased expression at the membrane compared to Kv7.3

Kv7.2mut acts in a dominant-negative manner to reduce Kv7 conductance

Cannabidiol acts on Kv7.x activation voltage to offset the effects of Kv7.2mut

Zhan et al., iScience 25, 105092
October 21, 2022
https://doi.org/10.1016/j.isci.2022.105092

iScience

CellPress
OPEN ACCESS

Article

Cannabidiol counters the effects of a dominant-negative pathogenic Kv7.2 variant

Xiaoqin Zhan,[1,2] Chris Drummond-Main,[2] Dylan Greening,[2] Jinjing Yao,[3,2] S.W.R. Chen,[3,2] J.P. Appendino,[1,5] P. Y. Billie Au,[1,4] and Ray W. Turner[1,2,6,*]

SUMMARY

Epilepsy and neurodevelopmental disorders can arise from pathogenic variants of KCNQ (Kv7) channels. A patient with developmental and epileptic encephalopathy exhibited an in-frame deletion of histidine 260 on Kv7.2. Coexpression of Kv7.2 mutant (mut) subunits with Kv7.3 invoked a decrease in current density, a depolarizing shift in voltage for activation, and a decrease in membrane conductance. Biotinylation revealed an increased level of surface Kv7.2mut compared to Kv7.3 with no change in total membrane protein expression. Super-resolution and FRET imaging confirmed heteromeric channel formation and a higher expression density of Kv7.2mut. Cannabidiol (1 μM) offset the effects of Kv7.2mut by inducing a hyperpolarizing shift in voltage for activation independent of CB1 or CB2 receptors. These data reveal that the ability for cannabidiol to reduce the effects of a pathogenic Kv7.2 variant supports its use as a potential therapeutic to reduce seizure activity.

INTRODUCTION

Pathogenic variants in the KCNQ (Kv7) family of voltage-gated potassium channels can disrupt cell and circuit function by modifying M current that promotes epilepsy and neurodevelopmental disorders (Gamal El-Din et al., 2021; Gilling et al., 2013; Jentsch, 2000). The Kv7.2, Kv7.3, and Kv7.5 isoforms are widely expressed in neurons and produce currents pivotal to controlling neuronal excitability near resting potentials (Baculis et al., 2020; Greene and Hoshi, 2016). Although Kv7.2 subunits are able to form homomeric channels in heterologous express systems and in the brain, they most often heteromerize with Kv7.3 subunits to mediate larger currents (Schwake et al., 2000; Springer et al., 2021). Kv7 mutations in epilepsy result in considerable phenotypic heterogeneity, ranging from the mild presentation like benign familial neonatal seizures (BFNS) to the more severe neonatal onset epileptic encephalopathy (NOEE) (Cooper et al., 2015; Vanoye et al., 2022). Many pathogenic Kv7 variants are missense substitutions that can affect channel function by changing voltage for activation (Va) (Miceli et al., 2013; Orhan et al., 2014), subcellular localization or expression (Abidi et al., 2015; Kim et al., 2018; Maljevic et al., 2011; Orhan et al., 2014), aberrant protein folding (Maljevic et al., 2011; Urrutia et al., 2021), or channel conductance (Gomis-Pérez et al., 2019; Orhan et al., 2014). For severe forms of epilepsy such as NOEE, pathogenic variants are often found in the voltage sensor and pore domains (S4-S6) and on the Kv7.2 C-terminus, although the molecular underpinnings that promote BFNS or NOEE phenotypes overlap (Nappi et al., 2020; Vanoye et al., 2022).

In this study, we assess a previously unreported variant in Kv7.2 in a proband with an in-frame deletion of histidine 260 (H260del) in the extracellular loop between S5 and the S6 transmembrane domains. The proband has a history of severe neurodevelopmental delays and drug-resistant epilepsy. Recordings in tsA-201 cells expressing Kv7 subunits with the H260del mutation (Kv7.2mut) show that it acts in a dominant-negative manner to substantially reduce Kv7 current through increased membrane expression of Kv7.2H260del, a shift in voltage dependence, and a decreased membrane conductance. Clinically, the proband eliminates seizures through cannabidiol (CBD)/THC treatment. When CBD (1 μM) was applied as a newly identified agonist of Kv7 channels (Incontro et al., 2021; Zhang et al., 2022) in tsA-201 cells coexpressing Kv7.2 wt + Kv7.2mut + Kv7.3, it rapidly induced a restorative negative shift in channel Va independent of any effects on CB1 or CB2 receptors. These findings identify the molecular basis for the effects of a Kv7.2 mutation and offer a potential means to alleviate symptoms in affected patients through low-dose CBD administration.

[1]Alberta Children's Hospital Research Institute, University of Calgary, Calgary, Alberta T2N 4N1, Canada

[2]Hotchkiss Brain Institute, University of Calgary, Calgary, Alberta T2N 4N1, Canada

[3]Libin Cardiovascular Research Institute, University of Calgary, Calgary, Alberta T2N 4N1, Canada

[4]Department of Medical Genetics, University of Calgary, Calgary, Alberta T2N 4N1, Canada

[5]Pediatric Department, Cumming School of Medicine, University of Calgary, Calgary, Alberta T2N 4N1, Canada

[6]Lead contact

*Correspondence: rwturner@ucalgary.ca

https://doi.org/10.1016/j.isci.2022.105092

RESULTS

Genetic analysis and patient background

The proband was born to a non-consanguineous couple after an uncomplicated pregnancy and delivered at term via repeated Caesarean section. As a neonate, she began demonstrating extension tonic stiffening of both arms and legs, lasting between 30 s and 5 min. This led to the diagnosis of early infantile epileptic encephalopathy suggestive of Ohtahara syndrome. Chromosome microarray was normal, but a clinical epilepsy gene panel done through Blueprint Genetics, encompassing 283 genes, identified a variant in KCNQ2, c.778_780del, p.His260del (NM_172107.3) that is absent from the GnomAD v2.1.1 database (https://gnomad.broadinstitute.org/, accessed Feb 14, 2022). Parental testing subsequently confirmed this variant occurred *de novo*. According to current ACMG variant classification guidelines, this variant was considered likely pathogenic (PS2, PM2); however, in-frame variants are less commonly reported in the literature in contrast to missense substitutions, and the direct impact of this variant on channel function was unknown (Richards et al., 2015).

At approximately 1 year of age, additional seizure types emerged. This included recurrent episodes of tonic-clonic convulsive status epilepticus, symmetrically involving arms and legs, and often with synchronous head and eye deviation that occurred very regularly every six weeks for 4–8 h each. For the first 7 years of life, seizures were drug-resistant, with multiple antiseizure medications trialled including phenobarbital, phenytoin, carbamazepine, topiramate, lamotrigine, clobazam, and levetiracetam. She had multiple PICU admissions until approximately 7 years of age. At that time, she was on lamotrigine and clobazam. MRI at 7 years old showed thinning of the corpus callosum and optic nerves but no other obvious anomalies. She was trialled on intravenous immunoglobulin at 7 years of age and had a favorable response with a reduction in seizure frequency and only one further episode. Between 8 and 11 years of age, she remained almost seizure free but had a recurrence at age 11 that evolved to general tonic-clonic convulsion. The proband also exhibited intellectual disability and dyskinetic cerebral palsy.

Her family started her on a 1:1 treatment of cannabidiol (CBD) and *trans*-Δ^9-tetrahydrocannabinol (THC) oil with good response, taking 200 mg (16.6 mg/kg) of 1:1 CBD and THC twice a day. At last assessment, at age 14, she had not had any clinical seizures for 3 years, with some additional reported reduction of spasticity and tremor and improved oral feeding and dexterity.

A Kv7.2H260 deletion mutation reduces Kv7 currents

To better understand the effects of Kv7.2H260del on brain activity, we conducted a series of electrophysiological and imaging studies at the single cell level to define its effects on homomeric and heteromeric channels that incorporate Kv7.3. It is known that Kv7.3 and Kv7.2 channels expressed in isolation produce only small amplitude currents. Kv7.3 normally increases the membrane expression of other Kv7 channel subunits and can invoke a hyperpolarizing shift in the voltage dependence for activation to increase current amplitude (Schwake et al., 2000; Springer et al., 2021). The Kv7.2H260del mutation is positioned in the external loop of the channel between transmembrane domains 5 and 6 (Figures 1A and 1B). To examine the influence of the H260del mutation on channel biophysical properties, we conducted whole cell patch clamp recordings in tsA-201 cells transiently transfected with wild-type (Kv7.2 wt) or mutant Kv7.2 (Kv7.2mut) cDNA, alone or in combination with Kv7.3. Kv7 current was pharmacologically isolated (see STAR Methods) and activated by a 1.5 s command pulse from a holding potential of −80–40 mV in steps of 10 mV (Figures 1C and 1D). Both Kv7.2 wt and Kv7.2 wt + Kv7.3 channel currents were as previously reported in presenting as a slow activating and non-inactivating current during the command pulse (Figure 1C) (Nappi et al., 2020). Kv7.2 wt current reached a peak amplitude of under ~2500 pA and Kv7.3 expressed alone produced even less current (451.2 ± 75.7 pA, n = 16) (Figure 1C). Coexpressing Kv7.2 + Kv7.3 cDNA to allow formation of heteromeric channels produced far greater current with peak amplitudes of ~6000 pA (Figures 1C and 1D). Current from Kv7.2mut expressed alone was dramatically reduced relative to those of Kv7.2 wt expressed alone (Figures 1C and 1D), with the current density (measured at 10 mV) being reduced from 119.2 ± 22.0 pA/pF (n = 10) for Kv7.2 wt to 7.5 ± 1.5 pA/pF (n = 6) for Kv7.2mut ($p = 0.0311$) (Figure 1E). Coexpressing Kv7.2mut + Kv7.3 also dramatically reduced channel current density from 285.2 ± 31.3 pA/pF (n = 16) for Kv7.2 wt + Kv7.3 to 20.3 ± 4.3 pA/pF for Kv7.2mut + Kv7.3 (n = 22; $p < 0.0001$) (Figure 1E).

As previous studies have shown that Kv7.2 mutations can shift the channel voltage dependence (Nappi et al., 2020), we examined the influence of H260del on voltage dependence for activation of Kv7.2 channels.

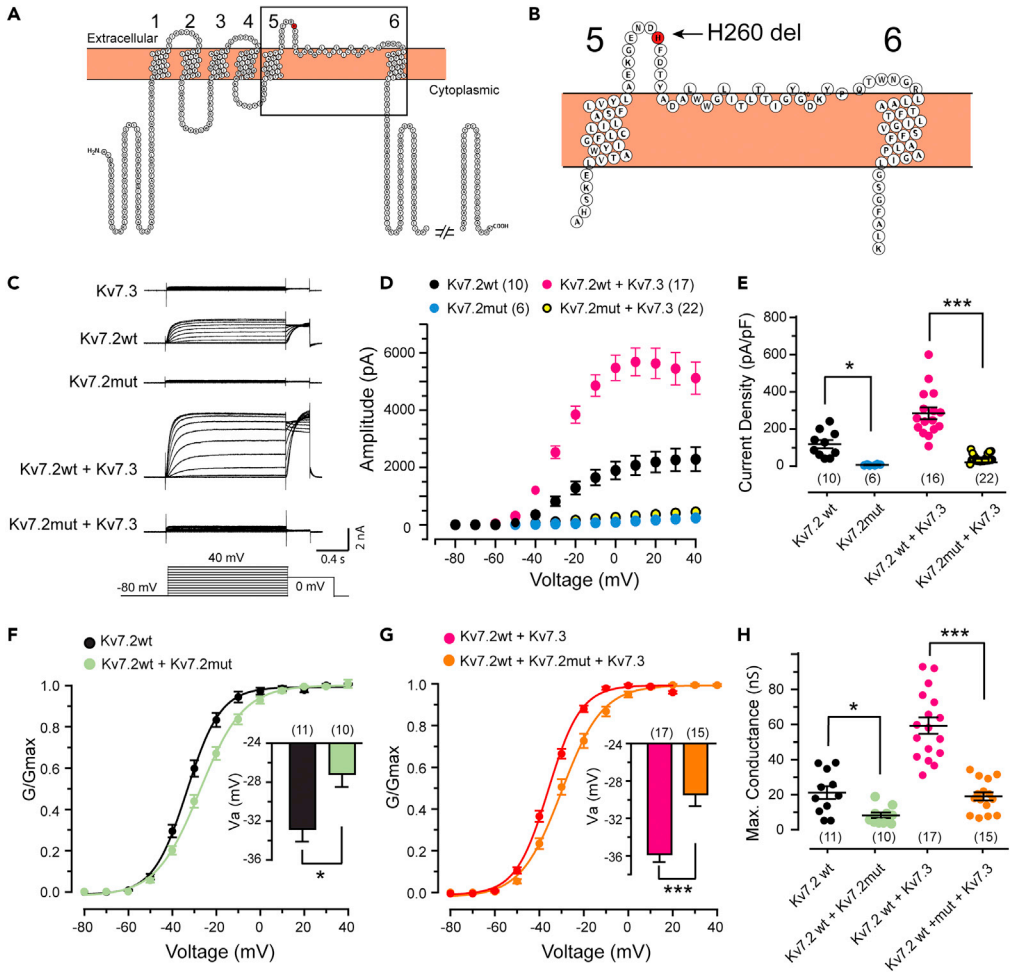

Figure 1. A Kv7.2 mutation reduces current amplitude of Kv7.2 + Kv7.3 channels by shifting voltage dependence and reducing channel conductance

(A and B) Schematic diagram of the Kv7.2 channel (A, Uniprot O43526) with 6 transmembrane domains (1–6) and the N- and C-termini positioned in the cytosol. A region of interest in (A) (box) is expanded in (B) to illustrate the position of a H260del mutation in the external membrane loop between transmembrane domains 5 and 6.

(C) Representative whole-cell recordings from tsA-201 cells with the indicated Kv7 channel subunits transiently expressed and depolarized from −80 mV to 40 mV in 10 mV steps followed by a step to 0 mV.

(D) Mean current amplitudes of the indicated Kv7 subunits when evoked with the protocol shown in (C). Sample numbers are shown in brackets.

(E) Mean-dot plots of current density (pA/pF measured at 10 mV) for whole-cell recordings of Kv7.2 wt or Kv7.2mut when expressed in tsA-201 cells alone ($p = 0.0311$) or when coexpressed with Kv7.3 ($p < 0.0001$, post hoc Tukey's test following two-way ANOVA).

(F and G) Conductance plots for the indicated expressed Kv7 channel subunits, with bar plots of mean Va (*insets*). The Kv7.2mut significantly shifts the channel activation curves in the depolarizing direction (F, $p = 0.007$; G, $p = 0.00017$, two sample Student's *t* test).

(H) Mean-dot plots for the indicated expressed Kv7 channel subunits show a reduction in maximal conductance when Kv7.2mut is coexpressed with either Kv7.2 wt ($p = 0.0323$) or with Kv7.2 wt + Kv7.3 ($p < 0.0001$, post hoc Tukey's test following two-way ANOVA).

All average values are mean ± SEM and number of cells provided in brackets. *$p < 0.05$, ***$p < 0.001$. Images in (A and B) were constructed with the online Protter tool (http://wlab.ethz.ch/protter/) based on UniProt entry number O43526. The C-terminus in (A) is truncated for display purposes.

We first determined the effects of Kv7.2mut on a heteromeric combination with Kv7.2 wt channels (1:1 ratio). Expressing Kv7.2mut shifted the steady-state activation curve measured for Kv7.2 wt current in the positive direction (Figure 2F), with the half-activation voltage (Va) shifted by 5.6 mV for Kv7.2mut + Kv7.2 wt

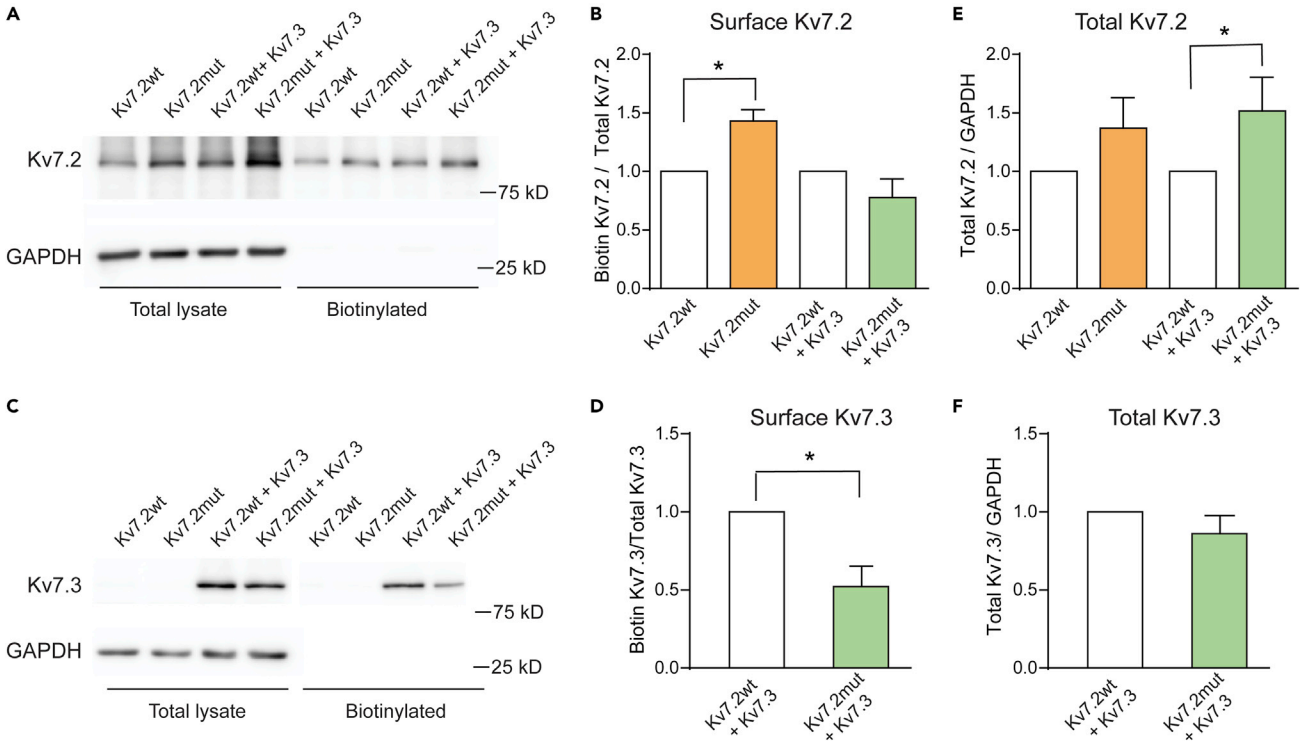

Figure 2. A Kv7.2H260del mutant changes the balance of surface expression of Kv7.2 and Kv7.3 subunits

(A-D) Transfected tsA201 cells were lysed after treatment with Sulfo-NHS-SS-biotin to identify surface proteins by immunocytochemical detection. Western blots of Kv7.2. (A and B) and Kv7.3 (C and D) in the total lysate and the biotinylated (cell membrane) fraction were probed with rabbit anti-Kv7.2 antibody and rabbit anti-Kv7.3 antibody, respectively. A clean biotinylated fraction of the lysate was confirmed with the absence of GAPDH in cell membrane samples. Bar graphs of mean values (B) for surface Kv7.2 presented as the ratio of biotinylated Kv7.2 to total Kv7.2 in different expression conditions reveals more Kv7.2 protein at the membrane in the Kv7.2mut transfected cells ($p = 0.021$, Mann-Whitney test, $n = 4$). D) Membrane Kv7.3 expression is decreased upon coexpression with Kv7.2mut ($p = 0.021$, Mann-Whitney test, $n = 4$).

(E and F) Total expression of Kv7.2mut was significantly increased when coexpressed with Kv7.3 (E) ($p = 0.0072$, Mann-Whitney test, $n = 5$), while the total level of Kv7.3 is not affected (F) ($p = 0.6558$, Mann-Whitney test, $n = 5$).

Data in bar plots of (E and F) are expressed in relation to GAPDH. Average values are mean ± SEM. *$p < 0.05$, Mann-Whitney test. N represents trials repeated.

heteromers relative to Kv7.2 wt homomers (Kv7.2 wt −32.8 ± 1.3, n = 11; Kv7.2mut + Kv7.2 wt −27.2 ± 1.3, n = 10; p = 0.007). A slightly larger rightward shift of 6.4 mV was measured when coexpressing Kv7.2mut + Kv7.2 wt + Kv7.3 (−29.4 ± 1.3, n = 15) relative to Kv7.2 wt + Kv7.3 (−35.8 ± 0.8, n = 17; p = 0.00017) (Figure 1G).

A rightward shift in voltage for activation will contribute to the observed effects of the Kv7.2mut isoform in reducing channel currents. The additional reduction in current density (Figure 1E) could reflect a shift in channel conductance or a change in membrane channel insertion. To address the potential for a change in conductance, we measured the maximum conductance on activation plots. When currents were normalized on conductance plots, the values differed by less than 5%. But comparing the values for absolute conductance showed that Kv7.2mut homomeric channels had a significantly lower maximum membrane channel conductance of 8.3 ± 1.6 nS (n = 10) compared to 21.2 ± 3.7 nS (n = 11) for Kv7.2 wt channels (p = 0.0323) (Figure 1H). Similarly, coexpressing Kv7.2mut + Kv7.3 wt significantly reduced the maximum membrane conductance from 59.3 ± 4.6 nS (n = 17) for Kv7.2 wt + Kv7.3 to 19.2 ± 2.4 nS for Kv7.2mut + Kv7.3 (n = 15; p < 0.0001, post-hoc Tukey's test following two-way ANOVA) (Figure 1H).

A Kv7.2H260 deletion mutation shifts the balance of Kv7 subunit expression at the membrane

To gain a more specific measure of how the H260del mutation affects membrane expression of Kv7 subunits, we conducted a biotinylation assay on tsA-201 cells expressing either Kv7.2 wt or Kv7.2mut with or without Kv7.3 coexpression. Surface Kv7.2 and Kv7.3 level was calculated as a ratio of biotinylated Kv7

subunits in the total cell lysates and then normalized to the wild-type condition. Semi-quantification of the membrane level of Kv7.2 subunits in the biotinylated membrane samples with Western blot revealed a significant increase in the membrane fraction of Kv7.2mut subunits compared to Kv7.2 wt (Figures 2A and 2B). The ratio of Kv7.2 in membrane fraction lysate to Kv7.2 in total lysate in Kv7.2mut expressing cells was 1.43 $\pm$ 0.10 (n = 4) times higher than that for Kv7.2 wt (p = 0.021) (Figures 2A and 2B). However, the membrane level of Kv7.2 in cells that also coexpressed Kv7.2mut and Kv7.3 was not significantly different from the wild-type channels (Figures 2A and 2B). The total Kv7.2 protein level showed a trend of increasing for the homomeric Kv7.2 channels, and was significantly increased in cells coexpressing Kv7.2mut + Kv7.3 channels compared to Kv7.2 wt + Kv7.3 (1.52 $\pm$ 0.13, n = 5, p = 0.00729) (Figure 2E). We also quantified the level of Kv7.3 on the membrane for tsA-201 cells coexpressing Kv7.2 wt or Kv7.2mut cDNA. In contrast to measures of Kv7.2 subunits, cells coexpressing Kv7.3 + Kv7.2mut exhibited a significant decrease in the level of Kv7.3 at the membrane (0.52 $\pm$ 0.13, n = 4, p = 0.02107) (Figures 2C and 2D) without affecting its total level (Figure 2F).

Together, these results reveal that coexpressing Kv7.mut with Kv7.3 subunits results in a significant increase in the level of membrane-associated Kv7.2mut subunits but a corresponding decrease in surface Kv7.3. The parallel increase in total Kv7.2mut membrane protein but not total Kv7.3 effectively shifts the balance of membrane expression for these two isoforms. The extent to which this corresponds to a shift in the stoichiometry of subunits assembled within heteromeric channels or a change in the extent of heteromeric vs homomeric channel expression cannot be determined from this dataset. However, an increased expression of Kv7.2mut subunits can be expected to contribute to the lower maximal conductance and right-shifted Va of channels detected electrophysiologically (Figures 1D–1F).

Super-resolution imaging supports heteromeric Kv7 channel formation with altered expression patterns

One possible explanation for the effects of an increase in Kv7.2mut expression on Kv7 current would be to interfere with the heteromeric assembly of subunits or their expression at the membrane. To further assess protein interactions, we used direct stochastic optical reconstruction microscopy (dSTORM) to image Kv7 immunolabels and quantify the degree of overlap of label emissions and the minimal distance between neighboring immunolabeled clusters. By combining dSTORM with total internal reflection fluorescence (TIRF) illumination, we could further restrict visualization of Kv7 immunolabels to within 150 nm of the coverslip surface to which cultured cells are attached. Kv7.2 subunits were detected directly with an anti-Kv7.2 antibody and Kv7.3 using an HA-tagged construct. The precision of resolution determined under our conditions reached 20–40 nm in the lateral plane. As such, the threshold for minimal cluster diameter was set at 40 nm, a size we expect reflects a signal from more than one subunit or channel.

Dual labeling of tsA-201 cells coexpressing Kv7.2 and Kv7.3 cDNAs revealed distinct fluorescent clusters either in isolation or positioned with enough proximity to exhibit overlap in the fluorescent signal emissions consistent with formation of heteromeric Kv7.2-Kv7.3 channels (Figures 3A–3D). Magnified regions of interest (ROI) further suggested a more extensive degree of overlap between Kv7.3 and Kv7.2mut compared to Kv7.3 and K7.2 wt subunits (Figures 3B–3D). Calculating the cluster density per unit area revealed a substantial difference in the absolute density of detected clusters, with 151 $\pm$ 15 clusters/μm^2 for Kv7.2 wt (n = 9) and 91 $\pm$ 3.4 clusters/μm^2 for Kv7.3 (n = 9; p = 0.0033) (Figure 3E). A similar difference in the density of clusters was apparent for the Kv7.2mut label (134 $\pm$ 14 clusters/μm^2; n = 9) compared to Kv7.3 (95.6 $\pm$ 4.9 clusters/μm^2; n = 9; p = 0.027) (Figure 3E). However, no significant differences were found between the number of Kv7.2 wt vs Kv7.2mut clusters (Kv7.2 wt, 151 $\pm$ 15 clusters/μm^2, n = 9; Kv7.2mut, 134 $\pm$ 14 clusters/μm^2, n = 9; p = 0.43) or between the ratios of Kv7.3 + Kv7.2 wt clusters (1.65 $\pm$ 0.13, n = 9) to that of Kv7.3 + Kv7.2mut clusters (1.43 $\pm$ 0.14, n = 9; p = 0.288). Quantification of immunolabeled clusters then indicated that both Kv7.2 wt and Kv7.2mut isoforms exhibit a higher level of expression compared to Kv7.3, and with similar relative levels for Kv7.2 wt/Kv7.3 to that of Kv7.2mut/Kv7.3 (Figure 3E).

To gain an estimate of the degree of colocalization, we calculated Manders's correlation coefficient to quantify the fractional overlap of one immunolabel emission upon the other. This analysis revealed a marked disparity in the overlap of Kv7.3 labels compared to Kv7.2 isoforms. Thus, a smaller percentage of the total intensity of Kv7.2 wt label overlapped with Kv7.3 (M2) compared to a large portion of Kv7.3 labels that overlapped with Kv7.2 wt (M1) (M1wt vs M2wt, n = 20; p = 6.29×10^{-8}) (Figure 3F). A similar difference was detected in the extent of overlap for the Kv7.2mut subunit with Kv7.3 (M2mut), in which a larger

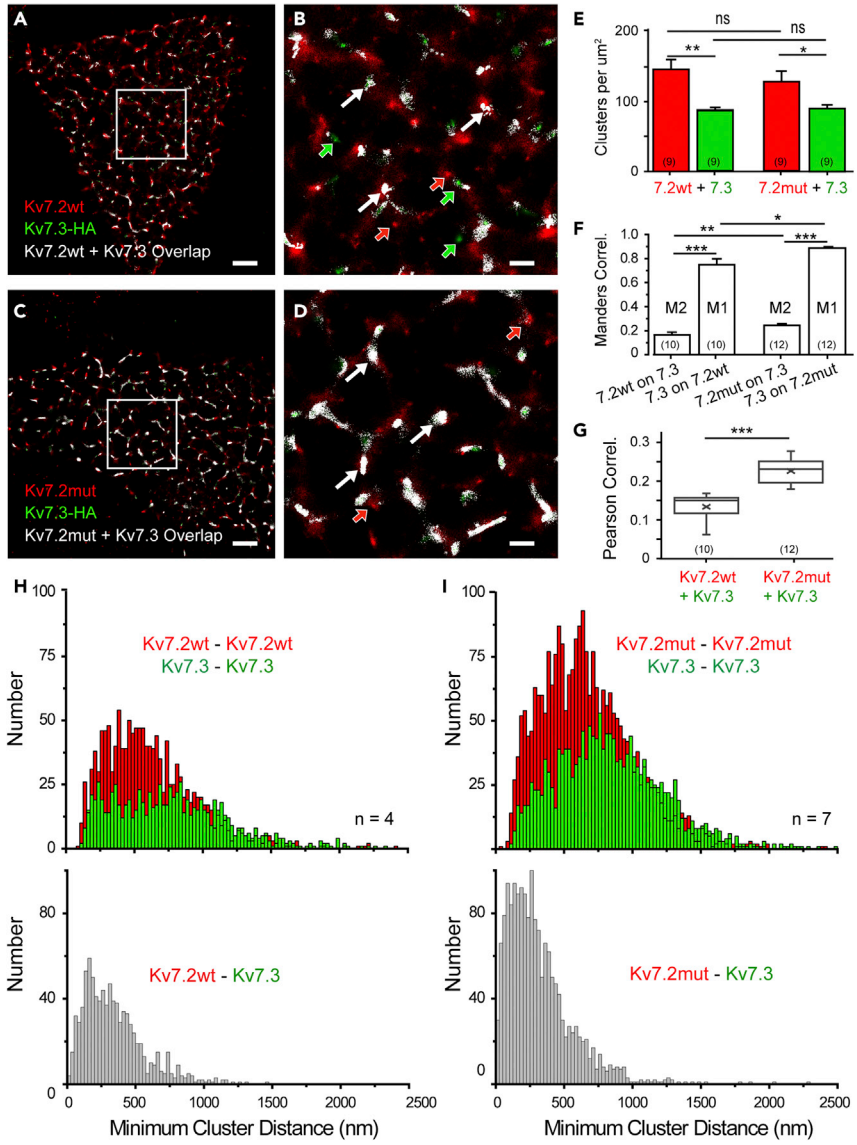

Figure 3. Kv7.2mut and Kv7.3 subunits exhibit strong colocalization in tsA-201 cells

(A–D) dSTORM-TIRF images of dual immunofluorescent labeling for the indicated pairs of expressed subunits at low power (A and C) and for representative ROIs (*boxes*) expanded in (B and D). Images of immunolabeled protein clusters are reconstructed from 6000 to 10000 aligned images, with locations of green and red pixel overlap shown as *white* labels. In (B and D), select cases of overlapping signals are indicated by *solid white arrows*, and isolated clusters by *red filled arrows* (Kv7.2 wt) and *green filled arrows* (Kv7.3).

(E) Bar plots of mean cluster density (number/μm^2) for the indicated pairs of coexpressed subunits.

(F) Bar plots of mean Manders' correlation coefficients to define the extent of overlap of immunofluorescent labels. M1 refers to the sum of Kv7.3 (green) label pixel intensity when any Kv7.2 (red) label intensity is present divided by total Kv7.3 (green) intensity, while M2 refers to the sum of red with green over total red intensity.

(G) Box-whisker plots of Pearson correlation coefficients to assess the extent of overlap of immunofluorescent labels. Measurements are derived by plotting red vs green channel intensity for every pixel and calculating a correlation statistic.

(H, I) Histogram plots of the minimal distance between nearest neighbor cluster centroids for the indicated pairs of coexpressed isoforms (bin width 25 nm).

Scale bars: (A and C) 2 μm, (B and D) 500 nm. All average values are mean ± SEM, *$p < 0.05$, **$p < 0.01$, ***$p < 0.001$, Student's *t* test. N represents the number of cells analyzed.

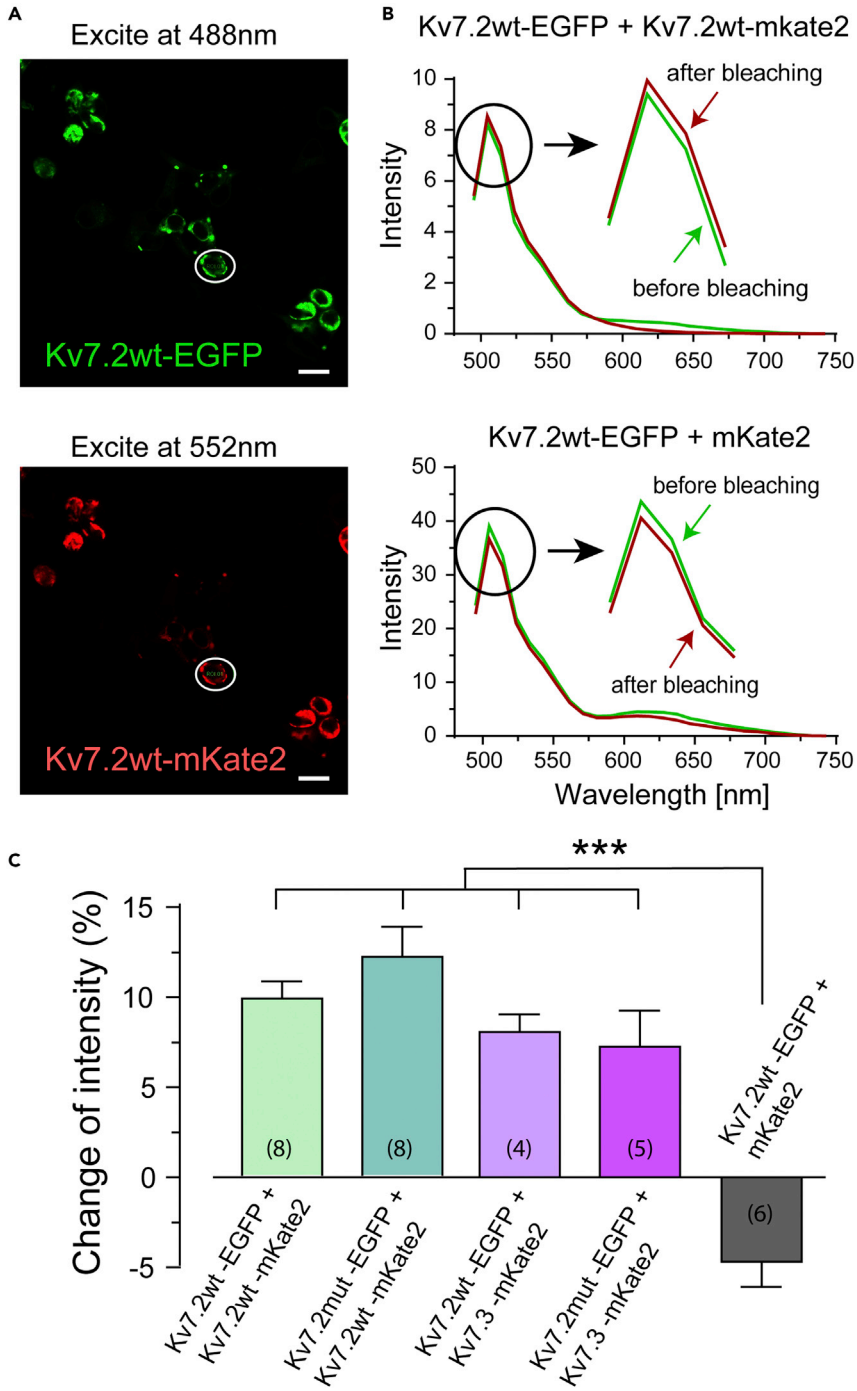

Figure 4. The Kv7.2mut subunit associates with Kv7.2 wt and Kv7.3 with nanometer proximities

(A) Confocal images of tsA-201 cells expressed with Kv7.2wt-EGFP + Kv7.2wt-mKate for detection of FRET. Only cells with both EGFP and mKate2 fluorescence are measured for the intensity of the EGFP channel after dye unmixing (see STAR Methods).

(B) Spectral images excited at 488 nm from two representative groups before and after photobleaching with 552 nm excitation. The intensity-wavelength plots of the ROI (circled) before and after photobleaching are presented on the right, with the *insets* showing the intensity scale for green fluorescence. An increase in the intensity of EGFP after photobleaching mKate in the cells expressing Kv7.2wt-EGFP + Kv7.2wt-mKate identifies FRET between EGFP and mKate.

(C) Quantification of the change of EGFP intensity under different expression combinations shows Kv7.2mut-EGFP FRETs with Kv7.2wt-mKate or Kv7.3-mKate, indicating a closeness, proximity of these channel subunits. Cells expressing

Figure 4. *Continued*
Kv7.2wt-EGFP and mKate2 serve as a non-FRET control which exhibited a decrease of ~5% EGFP intensity after photobleaching.
Scale bars in (A), 20 μm. All average values are mean ± SEM, *p < 0.05; **p < 0.01, ***p < 0.001, Student's *t* test. The sample sizes in the bar graphs represent the number of cells analyzed.

portion of Kv7.3 labels overlapped with Kv7.2mut (M1mut) (M1mut vs M2mut, n = 24; p = 2.2×10^{-16}). These results are in line with the noted cluster density disparities between Kv7.2mut and Kv7.3 (cf. Figures 4E and 4F). Comparison of either M1 or M2 between the Kv7.2 wt and Kv7.2mut condition showed significantly higher overlap when Kv7.3 was transfected with Kv7.2mut (M1wt vs M1mut, n = 22, p = 0.0039; M2wt vs M2mut, n = 22, p = 0.0017). These calculations suggest a higher incidence of colocalization between Kv7.2mut and Kv7.3 than for Kv7.2 wt and Kv7.3. This finding was further supported by higher Pearson correlation coefficients in cells cotransfected with Kv7.3 + Kv7.2mut than with Kv7.2 wt (n = 22; p = 2.312×10^{-6}) (Figure 3G).

The reasons for a difference in absolute cluster density (Figure 3E) and the extent of isoform overlap (Figures 3F and 3G) are unknown but suggests that the greater number of Kv7.2 clusters provide more than enough subunits to heteromerize with available Kv7.3 clusters. Analysis of the degree of overlap of signals further suggests that Kv7.2mut was more effective at associating with Kv7.3 than was Kv7.2 wt. A higher incidence of this presumed heteromeric formation was also evident visually in the number of overlapping fluorophore emissions (cf. Figures 3B–3D). However, we note that these interactions were not obligatory in that isolated clusters for a given subunit could also be detected.

dSTORM-TIRF imaging allows for calculation of the minimum distance to nearest neighbor cluster centroids. For this, we first coexpressed Kv7.2 wt and Kv7.3 cDNA and plotted histograms of the minimal distance between clusters of each isoform (Figure 3H). The histogram plot of minimal neighbor distance between Kv7.2 wt clusters (Kv7.2 wt - Kv7.2 wt) was moderately right-skewed with a distribution over 100–1600 nm and a peak ~500 nm (Sk_2 = 0.532; median = 565; K = 77. 2, n = 4). Similar results were found for histogram plots of the minimal distance between Kv7.3 clusters, with a distribution between 125 and 1750 nm and a peak ~800 nm (Sk_2 = 0.334; median = 737; K = 95.5, n = 4) (Figure 3H). In contrast, the histogram for minimal neighbor distances between clusters of Kv7.2 wt and Kv7.3 was strongly right-skewed with values between 0 and 950 nm and a peak ~150 nm (Sk_2 = 0.564; median = 300; K = 5.04, n = 4) (Figure 3H). A comparison of the minimal neighbor distances for cells coexpressing Kv7.2mut + Kv7.3 yielded similar results. Specifically, the histogram of minimal neighbor distance between Kv7.2mut clusters was moderately right-skewed over 125–1750 nm and peak at ~625 nm (Sk_2 = 0.435; median = 630; K = 53.4, n = 7) (Figure 3I). The histogram for minimal distances between Kv7.2mut and Kv7.3 was again strongly right-skewed over 0–975 nm and peak ~150 nm (Sk_2 = 0.655; median = 263; K = 10.0, n = 7) (cf. Figure 3I). The strong skew in minimal cluster distance histograms for Kv7.2 + Kv7.3 combinations is important in signifying a strong preferred association between these subunits, again as expected for successful heteromeric assembly of channel subunits.

Overall, these data support the electrophysiology on the ability for Kv7.2mut subunits to associate with Kv7.3 subunits at proximities consistent with formation of heteromeric channels. Yet, it is still important to acknowledge that dSTORM images restricted even to 150 nm depth of field through TIRF illumination could still report channels within the most superficial sites of the smooth ER or in transport to the membrane.

Kv7.2mut subunits associate at nanometer distance with Kv7.3 expected for heteromeric channel formation

The heteromeric assembly of specific Kv7 channel subunits into a functional channel can directly affect channel properties and the extent of incorporation at the membrane level (Maljevic et al., 2011; Schroeder et al., 1998; Schwake et al., 2000). Previous studies have shown that Kv7 subunits assemble close enough to promote fluorescence resonance energy transfer (FRET) when fluorescent-tagged channels are coexpressed in HEK293 cells (Bal et al., 2008). To test if Kv7.2mut affected the association between channel subunits, we used spectral-FRET to analyze Kv7 subunit interactions in tsA-201 cells (Wallrabe and Periasamy, 2005). EGFP was used as a donor molecule and mKate2 as an acceptor molecule and assessed using spectral confocal microscopy (Asmara et al., 2017).

Cells in the control and experimental groups were transfected with Kv7.2wt-EGFP + mKate2, and Kv7.2 wt/mut-EGFP + Kv7.3-mKate2, respectively. The vast majority of cells cotransfected with tagged channel subunits exhibited EGFP and mKate2 fluorescence when excited at 488 and 552 nm, respectively (Figure 4A). Spectral images were then taken with 488 nm laser and fluorophore channels were linearly unmixed. ROIs were selected to analyze the average intensity of EGFP before and after photobleaching the mKate2 at 552 nm to estimate the extent of energy transfer between EGFP and mKate2 (Wallrabe and Periasamy, 2005). The intensity of green fluorescence increased in the Kv7.2wt-EGFP + Kv7.2wt-mKate2 group after photobleaching mKate2 (9.8% $\pm$ 1.0%, n = 5, p = 1.9 $\times$ 10^{-5}) (Figures 4B and 4C), whereas the control group coexpressing Kv7.2wt-EGFP and mKate2 exhibited a slight decrease in EGFP intensity (4.7% $\pm$ 1.4%, n = 6) (Figures 4B and 4C). Together, these data verify the occurrence of FRET between Kv7.2wt-EGFP with Kv7.2wt-mKate2 as a heteromeric assembly of labeled subunits with spatial separations of <10 nm. For cells coexpressing the Kv7.2mut subunit, the intensity of EGFP also increased after photobleaching mKate2 (12.1% $\pm$ 1.7%, n = 6, p = 1.7 $\times$ 10^{-5}) (Figure 4C). Finally, a significant increase in fluorescence intensity was observed for coexpression of Kv7.2 wt or Kv7.2mut + Kv7.3 subunits (Kv7.2 wt + Kv7.3 7.9% $\pm$ 1.1%, n = 4, p = 2.1 $\times$ 10^{-4}; Kv7.2mut + Kv7.3 7.2% $\pm$ 2.0%, n = 5, p = 7.1 $\times$ 10^{-4}) (Figure 4C).

Taken together, these results suggest that Kv7.2mut does not impede the formation of Kv7.2-Kv7.3 heteromeric channels, as also suggested by dSTORM analysis. The lower membrane channel conductance measured with Kv7.2mut expression (Figure 1) thus does not reflect a loss of heteromeric channel assembly.

Cannabidiol rescues Kv7.2mut + Kv7.3 channel voltage dependence

Control of seizure activity has been increasingly gained through use of cannabinoids, with cannabidiol (CBD) specifically approved for clinical use (Pertwee et al., 2010; Watkins, 2019). This is important as our proband with the Kv7.2H260del reported improvement of epileptic seizures and some aspects of spasticity and tremor through administration of CBD:THC at 16.6 mg/kg twice a day. Moreover, a recent study reported that CBD can shift the voltage dependence of Kv7 channels expressed in CHO cells at concentrations as low as 30 nM, and increased the M-current recorded in cultured superior cervical ganglion or hippocampal neurons (Zhang et al., 2022). Endocannabinoids (eCBs) have also been shown capable of directly modifying Kv7 channel properties to regulate cell excitability (Incontro et al., 2021; Larsson et al., 2020b). Previous studies have established that CBD administered to subjects at 5–40 mg/kg/day produced peak plasma concentrations in the range of 0.29–1 μM (Cáceres Guido et al., 2021; Hwang et al., 2021), while a 120 mg/kg oral dose in rats could reach 12.6 μg/mL brain (40 μM) concentration (Deiana et al., 2012). We thus tested the effects of acute application of 1 μM CBD on the combination of Kv7.2mut + Kv7.2 wt + Kv7.3 subunits expressed in tsA-201 cells in the presence or absence of the combined CB1 blocker AM-251 (0.5 μM) and CB2 blocker SR 144528 (0.5 μM). We noted signs of washout effects of Kv7 currents in time-control recordings with a consistent rightward shift in Va and a more variable decrease in current amplitude during the 15 min of recording required for these tests. Given a variable degree of washout effects on current amplitude, we focused on the channel voltage dependence. Here, an equivalent time point comparison at 15 min revealed that CBD invoked a highly significant negative shift in Va from a baseline value in control recordings of Kv7.2 wt + Kv7.3 of -29.8 ± 1.25 mV to -35.6 ± 1.36 mV (n = 8; p = 1.06 $\times$ 10^{-5}) in CBD (Figure 5A). Notably, a net hyperpolarizing shift of -7.4 ± 1.3 mV (n = 8) in Va of the Kv7.2mut-containing channel in the presence of CBD was not significantly different from that of cells coexpressing Kv7.2 wt + Kv7.3 (Interaction between CBD and mutations on Va, p = 0.5146 by two-way ANOVA) (Figures 5A and 5B). Moreover, a net hyperpolarizing shift of -5.4 ± 0.4 mV (n = 5) in Va was induced by CBD in cells coexpressing Kv7.2mut + Kv7.2 + Kv7.3 in the presence of the CB1 and CB2 receptor blockers AM-251 (0.5 μM) and SR 144528 (0.5 μM) (Figure 5B), indicating the effects on Va did not involve CB receptor activity (Interaction between CBD and blocker on Va, p = 0.5935 by two-way ANOVA).

DISCUSSION

De novo missense Kv7.2 mutations are known to be a common cause of early-onset NOEEs, including the Ohtahara syndrome (Saitsu et al., 2012). The proband in this report with an in frame Kv7.2H260del mutation exhibits severe neurodevelopmental delays and NOEE that persisted since last assessment at age 14 years. The Kv7.2H260del is a previously undescribed variant located in the extracellular loop at aa 260 between S5 and S6, and is interpreted as "likely pathogenic" according to ACMG criteria due to its *de novo* status (PS1 criteria), and absence from normal population databases (PM2 criteria). The functional evidence provides direct support that this variant is causative for the clinical problems in this proband (PS3) (Richards et al., 2008, 2015). Some of the properties exhibited by this channel variant resembled that reported for other

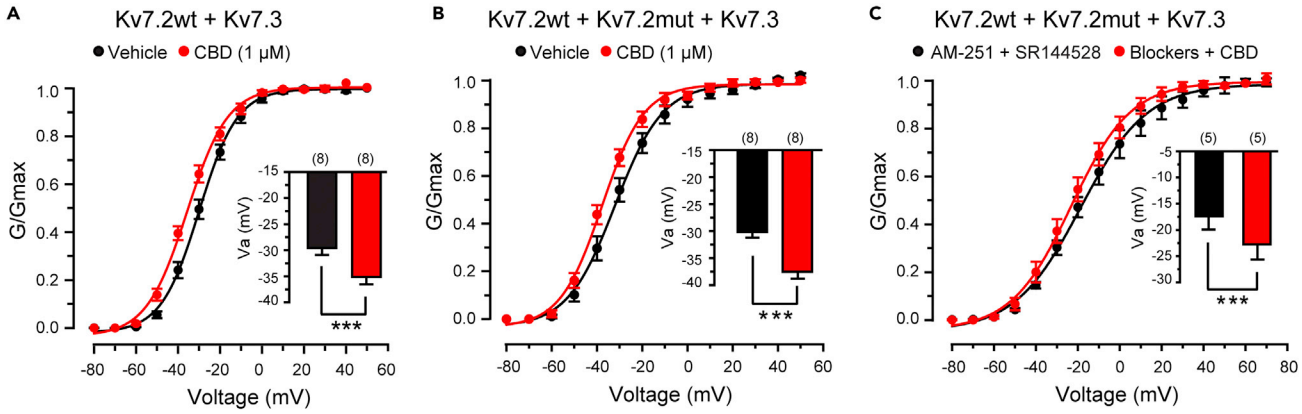

Figure 5. CBD reverses the voltage-dependent shift induced by Kv7.2mut. Shown are conductance plots to test the effects of bath applied 1 μM CBD on the indicated combinations of Kv7 subunits expressed in tsA-201 cells. The mean values of Va are indicated in the inset bar plots

(A and B) CBD applied to a combination of Kv7.2 wt + Kv7.3 (A) or Kv7.2 wt + Kv7.2mut + Kv7.3 (B) invokes a significant negative shift in Va.

(C) CBD (1 μM) induces a similar magnitude negative shift of Va for Kv7.2 wt + Kv7.2mut + Kv7.3 in the presence of the CB1/CB2 receptor blockers 0.5 μM AM-251 and 0.5 μM SR144528.

All average values are mean ± SEM and sample numbers provided in brackets. **p < 0.01, ***p < 0.001, Paired sample Student's *t* test. Number of cells was shown in brackets.

pathogenic Kv7.2 mutations (Nappi et al., 2020; Vanoye et al., 2022), including a dominant-negative effect that shifted the Va in a depolarizing direction and substantially reduced membrane current in tsA-201 cells. These properties were also reported in multiple Kv7 variants through a process of automatic patch analysis (Vanoye et al., 2022). The addition of biotinylation and dSTORM imaging here helped further reveal that Kv7.2H260del induced a shift in the balance between Kv7.2 and Kv7.3 subunits at the membrane despite no significant increase in total membrane protein expression. A detection of FRET between all subunits verified associations of <10 nm distance, suggesting no disruption of the ability to form heteromeric channels. With this information, a drastic reduction in whole-cell current density (pA/pF) in cells coexpressing Kv7.2mut + Kv7.3 subunits could be attributed to a depolarizing shift in Va and a decrease in maximal membrane conductance.

External loop mutations

Pathogenic variants found in Kv7.2 and Kv7.3 impact multiple possible residues that affect different aspects of channel function and lead variably to BFNS or more severe forms of epilepsy and encephalopathy (Milh et al., 2013; Nappi et al., 2020; Vanoye et al., 2022). The Kv7.2H260del examined here is positioned close to two other reported Kv7.2 mutations. These are also in the extracellular loop between S5 and S6 but at positions 258 (c.773A>G p.Asn258Ser, N258S) and 265 (c.793G>A p.Ala265Thr, A265T) (Cooper et al., 2015). In the case of the Kv7.2 N258S variant, the patient phenotype was BFNS (Yalçin et al., 2007). At the channel level, N258S presented as a dominant-negative factor that reduced current in Kv7.2 N258S + Kv7.3 channels, but with a reduced number of mutant channels at the membrane (Maljevic et al., 2011). No change in voltage dependence for activation was found, leading to a proposed defect in protein folding or trafficking (Maljevic et al., 2011). This differs from the Kv7.2H260del in which we detected a significant depolarizing shift in Va and no change in total Kv7 protein at the membrane. Although we cannot rule out the potential for a disorder in protein folding to account for the decrease in maximal membrane conductance in Kv7.2H260del + Kv7.3 channels, our results would suggest no specific disruption in ability for subunits to heteromerize, or for channels to traffick or insert at the membrane. Instead, the primary loss of function in Kv7.2H260del is reflected in a reduction in current through a shift in voltage for activation and a loss of membrane conductance not reported for the nearby N258S mutation.

The Kv7.2 A265T variant was detected in patients in some of the earliest studies linking Kv7.2 mutations with Ohtahara Syndrome (Milh et al., 2013; Saitsu et al., 2012; Weckhuysen et al., 2012), similar to the epilepsy phenotype described for our proband with Kv7.2H260del. The A265T variant also acted in a dominant-negative manner to suppress Kv7 current but failed to exhibit any change in voltage dependence

for activation or altered levels of surface expression (Milh et al., 2013), all effects that are opposite to that found for the Kv7.2H260del variant.

These comparisons support conclusions recently emphasized in a systematic comparison of Kv7.2 mutants using automated patch clamp where the net effect of a Kv7.2 mutation produced variable results (Vanoye et al., 2022). The current work now identifies differences at the channel level for mutations in the extracellular loop between S5 and S6 even when separated by only 2 amino acids, as highlighted by Kv7.2 N258S and H260del that lead to symptoms characteristic of BFNS or NOEE, respectively.

Therapeutic actions of CBD on a Kv7.2 mutation

A great deal of attention has been focused on achieving rescue of Kv7 channel function across the numerous pathogenic variants found in Kv7.2 or Kv7.3 subunits. A number of Kv7 activators have been reported that could provide potential recovery of function in Kv7.2 mutations (Borgini et al., 2021; Incontro et al., 2021; Kanyo et al., 2020; Larsson et al., 2020b; Vanoye et al., 2022), although non-specific actions or side effects have led to removal of some of these drugs from clinical use (Brickel et al., 2020). The proband with Kv7.2H260del had resolution of seizures through use of CBD:THC oil. The ability for CBD to act as an anti-epileptic treatment is well known (Williams and Stephens, 2020). CBD or eCBs were also recently reported to act as agonists for Kv7 channels in CHO, superior cervical ganglion, and hippocampal neurons (Incontro et al., 2021; Zhang et al., 2022). We therefore tested CBD in relation to Kv7 wild-type and Kv7.2mut subunits expressed in tsA-201 cells. Here, we found that 1 μM CBD induced ~ -5.7 mV hyperpolarizing shift in Va for coexpression of the Kv7.2 wt + Kv7.3 isoforms. While this is less than a shift of up to −17.5 mV reported for 1 μM CBD application in Zhang et al. (2022), it could reflect several differences that include cell lines (CHO vs tsA-201), CBD source, temperature, and drug application procedures. Importantly, we found that CBD also shifted the Va for Kv7.2mut + Kv7.2 + Kv7.3 by ~ -7 mV to −37.5 ± 1.3 mV compared to controls, a value that was not significantly different from that recorded after CBD application to cells coexpressing Kv7.2 wt + Kv7.3 ($p = 0.31$). These results are important in representing the first evidence that CBD can offset deficits in channel function caused by a Kv7.2 channel variant relevant to a patient's experience. Yet since CBD induced a hyperpolarizing shift in the Va of channels expressing either wild-type or mutant subunits (Figures 5A and 5B) (Zhang et al., 2022), we cannot conclude that its effects are specifically exerted on the mutant subunit. We would also interpret this to suggest no change in the binding efficacy of Kv7.2H260del-containing channels for CBD compared to wild-type channels, but this would need to be addressed through modeling (Incontro et al., 2021). Further work will also be needed to assess the potential for CBD to work in a similar fashion on channels incorporating the wide range of Kv7 mutations found in subjects (Cooper et al., 2015; Vanoye et al., 2022).

The mechanism(s) by which CBD offset the effects of Kv7.2mut on channel voltage dependence has not been established. In intact tissue, CBD is known to interact with a host of voltage- and ligand-gated channels that will modulate cell excitability and plasticity (Ghovanloo et al., 2018; Pertwee et al., 2010; Ross et al., 2008; Watkins, 2019). Since our recordings were conducted on principal subunits of Kv7 channels expressed in tsA-201 cells *in vitro*, many of these potential alternative sites of action will not be relevant here. Any potential actions of CBD on other potassium channels (Watkins, 2019) that might be expressed in tsA-201 cells are minimized given our blockade of a large spectrum of voltage- and calcium-gated potassium channels during recordings. It is known that CBD has a poor affinity for both CB1 and CB2 receptors but negatively modulates CB1 through an allosteric interaction (Laprairie et al., 2015). Our tests with CBD in the presence of the CB1and CB2 receptor blockers would indicate that the effects seen here do not involve CBD actions through these receptors. The ability to record effects by CBD within 20 min of drug application would be consistent with a direct interaction on Kv7 channels, as reported for eCBs and CBD (Incontro et al., 2021; Larsson et al., 2020b; Zhang et al., 2022). However, it is possible that CBD could interact with other receptors or channels in tsA-201 cells that could invoke other factors that modulate Kv7 channels (i.e. PiP2, PKC, calmodulin, arachidonic acid, and ERK1-2) (Borgini et al., 2021; Greene and Hoshi, 2016; Hudson et al., 2019; Larsson et al., 2020a).

The widespread influence of CBD on neural circuit function has identified a range of potential targets to reduce epileptic seizures in subjects (Baculis et al., 2020; Greene and Hoshi, 2016; Williams and Stephens, 2020). It is interesting that in structures such as neocortex and the hippocampus Kv7 channels can further

influence factors that range from morphological development through intrinsic excitability and circuit-wide theta frequency resonance (Baculis et al., 2020; Greene and Hoshi, 2016; Incontro et al., 2021; Peters et al., 2005). The current study together with recent reports of direct actions by eCBs and CBD on Kv7 channels (Incontro et al., 2021; Zhang et al., 2022) suggests that part of this influence could come about by modifying Kv7 channel function. Further work will also be required to determine the extent to which CBD acts specifically on Kv7 channels to account for anti-epileptic actions or autistic behaviors in subjects with Kv7 mutations.

Limitations of study

All data in the present study were obtained from Kv7 channel isoforms expressed in the tsA-201 cell line. While this approach can define the interactions possible between principal subunits of a channel, there could well be additional factors present in intact neurons that provide additional modulation of channel activity. One must also be cautious in directly extending conclusions drawn from results with CBD on channels expressed in isolation in tsA-201 cells to intact circuits.

STAR★METHODS

Detailed methods are provided in the online version of this paper and include the following:

- KEY RESOURCES TABLE
- RESOURCE AVAILABILITY
  - Lead contact
  - Materials availability
  - Data and code availability
- EXPERIMENTAL MODEL AND SUBJECT DETAILS
  - Cell lines
- METHOD DETAILS
  - Generation of cDNA constructs
  - Electrophysiology
  - Biotinylation
  - Immunostaining
  - Super-resolution imaging
  - Spectral-FRET imaging
- QUANTIFICATION AND STATISTICAL ANALYSES

ACKNOWLEDGMENTS

We gratefully acknowledge J. Forden and F. Visser of the Hotchkiss Brain Institute Molecular facility for technical assistance and H. Asmara for helpful discussions and support. This work was supported by a Canadian Institutes of Health Research Operating Grant (R.W.T.) (PJT156153).

AUTHOR CONTRIBUTIONS

Conception and design of the study: R.W.T., X.Z., C.D.-M., D.G., S.W.R., and P.Y.B.A. and J.P.A. conducted clinical analyses and medical management. Acquisition and analysis of data: C.D.-M. and X.Z. electrophysiology, X.Z. biotinylation, DG STORM-TIRF imaging, X.Z. and J.Y. FRET. Drafting of manuscript or figures: X.Z., C.D.-M., R.W.T., P.Y.B.A., and J.P.A.

DECLARATION OF INTERESTS

The authors declare no conflicts of interest.

INCLUSIVITY AND DIVERSITY

We support inclusive, diverse, and equitable conduct of research.

Received: June 2, 2022
Revised: August 17, 2022
Accepted: September 2, 2022
Published: October 21, 2022

REFERENCES

Abidi, A., Devaux, J.J., Molinari, F., Alcaraz, G., Michon, F.-X., Sutera-Sardo, J., Becq, H., Lacoste, C., Altuzarra, C., Afenjar, A., et al. (2015). A recurrent KCNQ2 pore mutation causing early onset epileptic encephalopathy has a moderate effect on M current but alters subcellular localization of Kv7 channels. Neurobiol. Dis. *80*, 80–92. https://doi.org/10.1016/j.nbd.2015.04.017.

Asmara, H., Micu, I., Rizwan, A.P., Sahu, G., Simms, B.A., Zhang, F.X., Engbers, J.D.T., Stys, P.K., Zamponi, G.W., and Turner, R.W. (2017). A T-type channel-calmodulin complex triggers alphaCaMKII activation. Mol. Brain *10*, 37. https://doi.org/10.1186/s13041-017-0317-8.

Baculis, B.C., Zhang, J., and Chung, H.J. (2020). The role of Kv7 channels in neural plasticity and behavior. Front. Physiol. *11*, 568667. https://doi.org/10.3389/fphys.2020.568667.

Bal, M., Zhang, J., Zaika, O., Hernandez, C.C., and Shapiro, M.S. (2008). Homomeric and heteromeric assembly of KCNQ (Kv7) K+ channels assayed by total internal reflection fluorescence/fluorescence resonance energy transfer and patch clamp analysis. J. Biol. Chem. *283*, 30668–30676. https://doi.org/10.1074/jbc.M805216200.

Bolte, S., and Cordelières, F.P. (2006). A guided tour into subcellular colocalization analysis in light microscopy. J. Microsc. *224*, 213–232. https://doi.org/10.1111/j.1365-2818.2006.01706.x.

Borgini, M., Mondal, P., Liu, R., and Wipf, P. (2021). Chemical modulation of Kv7 potassium channels. RSC Med. Chem. *12*, 483–537. https://doi.org/10.1039/d0md00328j.

Brickel, N., Hewett, K., Rayner, K., McDonald, S., De'Ath, J., Daniluk, J., Joshi, K., Boll, M.C., Tiamkao, S., Vorobyeva, O., and Cooper, J. (2020). Safety of retigabine in adults with partial-onset seizures after long-term exposure: focus on unexpected ophthalmological and dermatological events. Epilepsy Behav. *102*, 106580. https://doi.org/10.1016/j.yebeh.2019.106580.

Cáceres Guido, P., Riva, N., Caraballo, R., Reyes, G., Huaman, M., Gutierrez, R., Agostini, S., Fabiana Delaven, S., Pérez Montilla, C.A., García Bournissen, F., and Schaiquevich, P. (2021). Pharmacokinetics of cannabidiol in children with refractory epileptic encephalopathy. Epilepsia *62*, e7–e12. https://doi.org/10.1111/epi.16781.

Celikoglu, A., and Tirnakli, U. (2018). Skewness and kurtosis analysis for non-Gaussian distributions. Phys. Stat. Mech. Appl. *499*, 325–334.

Cooper, E.C., Taglialatela, M., Weckhuysen, S., and Joshi, N. (2015). Rational intervention for KCNQ2/3 epileptic encephalopathy. The Rikee Project. https://www.rikee.org/.

Deiana, S., Watanabe, A., Yamasaki, Y., Amada, N., Arthur, M., Fleming, S., Woodcock, H., Dorward, P., Pigliacampo, B., Close, S., et al. (2012). Plasma and brain pharmacokinetic profile of cannabidiol (CBD), cannabidivarine (CBDV), Δ^9-tetrahydrocannabivarin (THCV) and cannabigerol (CBG) in rats and mice following oral and intraperitoneal administration and CBD action on obsessive-compulsive behaviour. Psychopharmacology *219*, 859–873. https://doi.org/10.1007/s00213-011-2415-0.

Gamal El-Din, T.M., Lantin, T., Tschumi, C.W., Juarez, B., Quinlan, M., Hayano, J.H., Li, J., Zweifel, L.S., and Catterall, W.A. (2021). Autism-associated mutations in KV7 channels induce gating pore current. Proc. Natl. Acad. Sci. USA *118*. e2112666118. https://doi.org/10.1073/pnas.2112666118.

Ghovanloo, M.-R., Shuart, N.G., Mezeyova, J., Dean, R.A., Ruben, P.C., and Goodchild, S.J. (2018). Inhibitory effects of cannabidiol on voltage-dependent sodium currents. J. Biol. Chem. *293*, 16546–16558. https://doi.org/10.1074/jbc.RA118.004929.

Gilling, M., Rasmussen, H.B., Calloe, K., Sequeira, A.F., Baretto, M., Oliveira, G., Almeida, J., Lauritsen, M.B., Ullmann, R., Boonen, S.E., et al. (2013). Dysfunction of the heteromeric KV7.3/KV7.5 potassium channel is associated with autism spectrum disorders. Front. Genet. *4*, 54. https://doi.org/10.3389/fgene.2013.00054.

Gomis-Pérez, C., Urrutia, J., Marcé-Grau, A., Malo, C., López-Laso, E., Felipe-Rucián, A., Raspall-Chaure, M., Macaya, A., and Villarroel, A. (2019). Homomeric Kv7.2 current suppression is a common feature in KCNQ2 epileptic encephalopathy. Epilepsia *60*, 139–148. https://doi.org/10.1111/epi.14609.

Greene, D.L., and Hoshi, N. (2017). Modulation of Kv7 channels and excitability in the brain. Cell. Mol. Life Sci. *74*, 495–508. https://doi.org/10.1007/s00018-016-2359-y.

Hudson, R., Renard, J., Norris, C., Rushlow, W.J., and Laviolette, S.R. (2019). Cannabidiol counteracts the psychotropic side-effects of Δ-9-tetrahydrocannabinol in the ventral Hippocampus through bidirectional control of ERK1-2 phosphorylation. J. Neurosci. *39*, 8762–8777. https://doi.org/10.1523/JNEUROSCI.0708-19.2019.

Hwang, S., Lee, D.Y., Cho, J.-Y., Chung, J.-Y., Jang, I.-J., Yu, K.-S., and Lee, S. (2021). Pharmacokinetics, tolerability and pharmacogenetics of DA-8031 after multiple ascending doses in healthy male subjects. Drug Des. Devel. Ther. *15*, 2375–2384. https://doi.org/10.2147/DDDT.S309763.

Incontro, S., Sammari, M., Azzaz, F., Inglebert, Y., Ankri, N., Russier, M., Fantini, J., and Debanne, D. (2021). Endocannabinoids tune intrinsic excitability in O-LM interneurons by direct modulation of postsynaptic Kv7 channels. J. Neurosci. *41*, 9521–9538. https://doi.org/10.1523/JNEUROSCI.1279-21.2021.

Jentsch, T.J. (2000). Neuronal KCNQ potassium channels:physiology and role in disease. Nat. Rev. Neurosci. *1*, 21–30. https://doi.org/10.1038/35036198.

Kanyo, R., Wang, C.K., Locskai, L.F., Li, J., Allison, W.T., and Kurata, H.T. (2020). Functional and behavioral signatures of Kv7 activator drug subtypes. Epilepsia *61*, 1678–1690. https://doi.org/10.1111/epi.16592.

Kim, E.C., Zhang, J., Pang, W., Wang, S., Lee, K.Y., Cavaretta, J.P., Walters, J., Procko, E., Tsai, N.-P., and Chung, H.J. (2018). Reduced axonal surface expression and phosphoinositide sensitivity in Kv7 channels disrupts their function to inhibit neuronal excitability in Kcnq2 epileptic encephalopathy. Neurobiol. Dis. *118*, 76–93. https://doi.org/10.1016/j.nbd.2018.07.004.

Laprairie, R.B., Bagher, A.M., Kelly, M.E.M., and Denovan-Wright, E.M. (2015). Cannabidiol is a negative allosteric modulator of the cannabinoid CB1 receptor. Br. J. Pharmacol. *172*, 4790–4805. https://doi.org/10.1111/bph.13250.

Larsson, J.E., Frampton, D.J.A., and Liin, S.I. (2020a). Polyunsaturated fatty acids as modulators of KV7 channels. Front. Physiol. *11*, 641. https://doi.org/10.3389/fphys.2020.00641.

Larsson, J.E., Karlsson, U., Wu, X., and Liin, S.I. (2020b). Combining endocannabinoids with retigabine for enhanced M-channel effect and improved KV7 subtype selectivity. J. Gen. Physiol. *152*. e202012576. https://doi.org/10.1085/jgp.202012576.

Maljevic, S., Naros, G., Yalçin, Ö., Blazevic, D., Loeffler, H., Cağlayan, H., Steinlein, O.K., and Lerche, H. (2011). Temperature and pharmacological rescue of a folding-defective, dominant-negative KV 7.2 mutation associated with neonatal seizures. Hum. Mutat. *32*, E2283–E2293. https://doi.org/10.1002/humu.21554.

Malkusch, S., and Heilemann, M. (2016). Extracting quantitative information from single-molecule super-resolution imaging data with LAMA - LocAlization Microscopy Analyzer. Sci. Rep. *6*, 34486. https://doi.org/10.1038/srep34486.

Miceli, F., Soldovieri, M.V., Ambrosino, P., Barrese, V., Migliore, M., Cilio, M.R., and Taglialatela, M. (2013). Genotype–phenotype correlations in neonatal epilepsies caused by mutations in the voltage sensor of Kv7.2 potassium channel subunits. Proc. Natl. Acad. Sci. USA *110*, 4386–4391. https://doi.org/10.1073/pnas.1216867110.

Milh, M., Boutry-Kryza, N., Sutera-Sardo, J., Mignot, C., Auvin, S., Lacoste, C., Villeneuve, N., Roubertie, A., Heron, B., Carneiro, M., et al. (2013). Similar early characteristics but variable neurological outcome of patients with a de novo mutation of KCNQ2. Orphanet J. Rare Dis. *8*, 80. https://doi.org/10.1186/1750-1172-8-80.

Nappi, P., Miceli, F., Soldovieri, M.V., Ambrosino, P., Barrese, V., and Taglialatela, M. (2020). Epileptic channelopathies caused by neuronal Kv7 (KCNQ) channel dysfunction. Pflugers Arch. *472*, 881–898. https://doi.org/10.1007/s00424-020-02404-2.

Orhan, G., Bock, M., Schepers, D., Ilina, E.I., Reichel, S.N., Löffler, H., Jezutkovic, N., Weckhuysen, S., Mandelstam, S., Suls, A., et al. (2014). Dominant-negative effects of KCNQ2 mutations are associated with epileptic encephalopathy. Ann. Neurol. *75*, 382–394. https://doi.org/10.1002/ana.24080.

Pertwee, R.G., Howlett, A.C., Abood, M.E., Alexander, S.P.H., Di Marzo, V., Elphick, M.R., Greasley, P.J., Hansen, H.S., Kunos, G., Mackie,

K., et al. (2010). International union of basic and clinical pharmacology. LXXIX. Cannabinoid receptors and their ligands: beyond CB_1 and CB_2. Pharmacol. Rev. *62*, 588–631. https://doi.org/10.1124/pr.110.003004.

Peters, H.C., Hu, H., Pongs, O., Storm, J.F., and Isbrandt, D. (2005). Conditional transgenic suppression of M channels in mouse brain reveals functions in neuronal excitability, resonance and behavior. Nat. Neurosci. *8*, 51–60. https://doi.org/10.1038/nn1375.

Richards, C.S., Bale, S., Bellissimo, D.B., Das, S., Grody, W.W., Hegde, M.R., Lyon, E., and Ward, B.E.; Molecular Subcommittee of the ACMG Laboratory Quality Assurance Committee (2008). ACMG recommendations for standards for interpretation and reporting of sequence variations: revisions 2007. Genet. Med. *10*, 294–300. https://doi.org/10.1097/GIM.0b013e31816b5cae.

Richards, S., Aziz, N., Bale, S., Bick, D., Das, S., Gastier-Foster, J., Grody, W.W., Hegde, M., Lyon, E., Spector, E., et al.; ACMG Laboratory Quality Assurance Committee (2015). Standards and guidelines for the interpretation of sequence variants: a joint consensus recommendation of the American college of medical Genetics and genomics and the association for molecular pathology. Genet. Med. *17*, 405–424. https://doi.org/10.1038/gim.2015.30.

Ross, H.R., Napier, I., and Connor, M. (2008). Inhibition of recombinant human T-type calcium channels by Delta9-tetrahydrocannabinol and cannabidiol. J. Biol. Chem. *283*, 16124–16134. https://doi.org/10.1074/jbc.M707104200.

Sahu, G., Asmara, H., Zhang, F.X., Zamponi, G.W., and Turner, R.W. (2017). Activity-dependent facilitation of CaV1.3 calcium channels promotes KCa3.1 activation in hippocampal neurons. J. Neurosci. *37*, 11255–11270. https://doi.org/10.1523/JNEUROSCI.0967-17.2017.

Sahu, G., Wazen, R.-M., Colarusso, P., Chen, S.R.W., Zamponi, G.W., and Turner, R.W. (2019). Junctophilin proteins tether a cav1-RyR2-KCa3.1 tripartite complex to regulate neuronal excitability. Cell Rep. *28*, 2427–2442.e6. https://doi.org/10.1016/j.celrep.2019.07.075.

Saitsu, H., Kato, M., Koide, A., Goto, T., Fujita, T., Nishiyama, K., Tsurusaki, Y., Doi, H., Miyake, N., Hayasaka, K., and Matsumoto, N. (2012). Whole exome sequencing identifies KCNQ2 mutations in Ohtahara syndrome. Ann. Neurol. *72*, 298–300. https://doi.org/10.1002/ana.23620.

Schroeder, B.C., Kubisch, C., Stein, V., and Jentsch, T.J. (1998). Moderate loss of function of cyclic-AMP-modulated KCNQ2/KCNQ3 K+ channels causes epilepsy. Nature *396*, 687–690. https://doi.org/10.1038/2536.

Schwake, M., Pusch, M., Kharkovets, T., and Jentsch, T.J. (2000). Surface expression and single channel properties of KCNQ2/KCNQ3, M-type K+ channels involved in epilepsy. J. Biol. Chem. *275*, 13343–13348. https://doi.org/10.1074/jbc.275.18.13343.

Springer, K., Varghese, N., and Tzingounis, A.V. (2021). Flexible stoichiometry: implications for KCNQ2- and KCNQ3-associated neurodevelopmental disorders. Dev. Neurosci. *43*, 191–200. https://doi.org/10.1159/000515495.

Urrutia, J., Aguado, A., Gomis-Perez, C., Muguruza-Montero, A., Ballesteros, O.R., Zhang, J., Nuñez, E., Malo, C., Chung, H.J., Leonardo, A., et al. (2021). An epilepsy-causing mutation leads to co-translational misfolding of the Kv7.2 channel. BMC Biol. *19*, 109. https://doi.org/10.1186/s12915-021-01040-1.

Vanoye, C.G., Desai, R.R., Ji, Z., Adusumilli, S., Jairam, N., Ghabra, N., Joshi, N., Fitch, E., Helbig, K.L., McKnight, D., et al. (2022). High-throughput evaluation of epilepsy-associated KCNQ2 variants reveals functional and pharmacological heterogeneity. JCI Insight *7*, e156314. https://doi.org/10.1172/jci.insight.156314.

Wallrabe, H., and Periasamy, A. (2005). Imaging protein molecules using FRET and FLIM microscopy. Curr. Opin. Biotechnol. *16*, 19–27. https://doi.org/10.1016/j.copbio.2004.12.002.

Watkins, A.R. (2019). Cannabinoid interactions with ion channels and receptors. Channels *13*, 162–167. https://doi.org/10.1080/19336950.2019.1615824.

Weckhuysen, S., Mandelstam, S., Suls, A., Audenaert, D., Deconinck, T., Claes, L.R.F., Deprez, L., Smets, K., Hristova, D., Yordanova, I., et al. (2012). KCNQ2 encephalopathy: emerging phenotype of a neonatal epileptic encephalopathy. Ann. Neurol. *71*, 15–25. https://doi.org/10.1002/ana.22644.

Williams, C.M., and Stephens, G.J. (2020). Development of cannabidiol as a treatment for severe childhood epilepsies. Br. J. Pharmacol. *177*, 5509–5517. https://doi.org/10.1111/bph.15274.

Yalçin, O., Cağlayan, S.H., Saltik, S., Cokar, O., Ağan, K., Dervent, A., and Steinlein, O.K. (2007). A novel missense mutation (N258S) in the KCNQ2 gene in a Turkish family afflicted with benign familial neonatal convulsions (BFNC). Turk. J. Pediatr. *49*, 385–389.

Yao, J., Sun, B., Institoris, A., Zhan, X., Guo, W., Song, Z., Liu, Y., Hiess, F., Boyce, A.K.J., Ni, M., et al. (2020). Limiting RyR2 open time prevents Alzheimer's disease-related neuronal hyperactivity and memory loss but not β-amyloid accumulation. Cell Rep. *32*, 108169. https://doi.org/10.1016/j.celrep.2020.108169.

Zhang, H.-X.B., Heckman, L., Niday, Z., Jo, S., Fujita, A., Shim, J., Pandey, R., Al Jandal, H., Jayakar, S., Barrett, L.B., et al. (2022). Cannabidiol activates neuronal Kv7 channels. Elife *11*, e73246. https://doi.org/10.7554/eLife.73246.

Zhan, X., Asmara, H., Cheng, N., Sahu, G., Sanchez, E., Zhang, F.-X., Zamponi, G.W., Rho, J.M., and Turner, R.W. (2020). FMRP(1-297)-tat restores ion channel and synaptic function in a model of Fragile X syndrome. Nat. Commun. *11*, 2755. https://doi.org/10.1038/s41467-020-16250-4.

STAR★METHODS

KEY RESOURCES TABLE

REAGENT or RESOURCE	SOURCE	IDENTIFIER
Antibodies		
rabbit anti-Kv7.2	Cell Signaling Technology	Cat#14752 (clone D9L5S); RRID: AB_2798597
rabbit anti-kv7.3	Alomone	Cat#APC-051; RRID: AB_2040103
mouse anti-GAPDH	Invitrogen	Cat#39-8600 (clone ZG003); RRID: AB_2533438
HRP conjugated goat anti-mouse IgG	Invitrogen	Cat#62-6520; RRID: AB_2533947
HRP conjugated donkey anti-rabbit IgG	Cytiva	Cat# NA9340-1ml, RRID:AB_772191
Alexa Fluor-647 conjugated donkey $F(ab)_2$ anti-rabbit IgG	Jackson Immuno Research	Cat#711-606-152; RRID: AB_2340625
Cy-3 conjugated goat $F(ab)_2$ anti-mouse IgG	Jackson Immuno Research	Cat#115-166-146; RRID: AB_2338708
Chemicals, peptides, and recombinant proteins		
cannabidiol (CBD)	Sigma-Aldrich	Cat# C-045-1mL; CAS# 13956-29-1
AM-251	Tocris	Cat# 1117; CAS# 183232-66-8
SR144528	Sigma-Aldrich	Cat# SML1899-5MG; CAS# 192703-06-3
Critical commercial assays		
Q5 Site-directed mutagenesis kit	New England Biolabs	Cat# E0554S
Sulfo NHS-SS-Biotin	Thermo Fisher	Cat# PG82077
streptavidin agarose beads	Thermo Fisher	Cat# 20359
TetraSpek Microspheres	Thermo Fisher	Cat# T7279
Deposited data		
Raw and analyzed data, western blot images	This paper	10.6084/m9.figshare.20510907
Experimental models: Cell lines		
Human: tsA-201 cells	Sigma-Aldrich	Cat#85120602
Oligonucleotides		
Kv7.2mutation forward primer: TTTGACACCTACGCGGAT	This paper	N/A
Kv7.2mutation reverse primer: GTCGTTCTCCCCCTTCTC	This paper	N/A
Add EGFP tag to Kv7.2 wt and Kv7.2mut, forward primer: GATGATACGCGTACGC GGCCGCTCGAGATGGTGAGCAAGGGCGAGG	This paper	N/A
Add EGFP tag to Kv7.2 wt and Kv7.2mut, reverse primer: GATGATCCCGGGATCTGTTCAGGAAACAGCTATGACC GCGGCCGGCCGTCTAGCTACTAGCTAGTCGAGATCTGAG	This paper	N/A
Recombinant DNA		
Kv7.2 human ORF plasmid	Origene	RC212932
Kv7.3 human ORF plasmid	Origene	RC218739
Kv7.2-EGFP plasmid	This paper	N/A
Kv7.2H250del plasmid	This paper	N/A
Kv7.2H250del-EGFP plasmid	This paper	N/A
Kv7.3-mKate2 plasmid	This paper	N/A
Kv7.2-mKate2 plasmid	This paper	N/A
Kv7.3-HA	This paper	N/A

(*Continued on next page*)

Continued

REAGENT or RESOURCE	SOURCE	IDENTIFIER
Software and algorithms		
pClamp 10.6	Molecular Devices	https://moldevkb.blob.core.windows.net/kb01/software/cns/pclamp/10/pCLAMP_10_7_0.exe
Image Lab 6.1	Bio-Rad	https://www.bio-rad.com/en-ca/product/image-lab-software?ID=KRE6P5E8Z
ImageJ	NIH	https://imagej.nih.gov/ij/download.html
Localization Microscopy Analyzer (LAMA)	Malkusch and Heilemann (2016)	http://share.smb.uni-frankfurt.de/index.php/software-menue/lama
MATLAB	MathWorks	https://www.mathworks.com/products/matlab.html
Origin 8.0	OriginLab	https://www.originlab.com/
R		https://www.r-project.org/
Graphpad Prism 6	Graphpad Software	https://www.graphpad.com/

RESOURCE AVAILABILITY

Lead contact

Further information and requests for resources and reagents should be directed to and will be fulfilled by the lead contact, Ray W Turner (rwturner@ucalgary.ca).

Materials availability

- All materials will be made available upon reasonable request.
- This study did not generate new unique reagents.

Data and code availability

- Data and original western blot images have been deposited at Figshare and are publicly available as of the date of publication. DOI is listed in the Key resources table. Microscopy data reported in this paper will be shared by the lead contact upon request.
- This paper does not report original code.
- Any additional information required to reanalyze the data reported in this paper is available from the lead contact upon request.

EXPERIMENTAL MODEL AND SUBJECT DETAILS

Cell lines

The tsA-201 cell line derived from Human Embryonic Kidney cells from a female subject were purchased from Sigma-Aldrich and maintained (Sahu et al., 2017; Zhan et al., 2020). Cells were maintained in DMEM supplemented with 10% heat inactivated fetal calf serum and 1% penicillin-streptomycin at 37°C under 5% CO2 and splitted by trypsinization to plate at a density of 30–50% (patch-clamp and imagining) or 50–70% (protein assays) before transfecting with cDNAs overnight with the calcium phosphate-based method. EGFP cDNA was also transiently transfected (1 μg) as a transfection marker, 4 μg cDNA was used if only one Kv7 channel subunit was expressed, and 2 μg of each Kv7 subunit when more than 2 subunits were transfected. For biotinylation tests 2 μg of Kv7.2 or Kv7.3 cDNA was used. Cells were maintained at 32°C after transfection before being used.

METHOD DETAILS

Generation of cDNA constructs

Myc-tagged Kv7.2 (NM_172107, Origene, RC212932) and Kv7.3 (NM_004519, Origene, RC218739) in pCMV6-Entry vector were used for expression and as templates. The Kv7.2mut was generated with the Q5 Site-Directed Mutagenesis Kit (New England Biolabs, MA, USA, Cat. No. E0554S) with primers specified

in the Key resources table. EGFP and mKate2 tagged constructs were made by replacing myc tag in Kv7.2 wt or Kv7.2*mut* using the MluI and SacII restriction sites or in Kv7.3 using the XhoI and XmaI restriction sites. Primers were provided as in the Key resources table. All constructs were verified with restriction enzyme mapping and Sanger sequencing.

Electrophysiology

Whole-cell patch clamp recordings were obtained of Kv7 channels transiently transfected into tsA-201 cells plated onto glass coverslips (Sahu et al., 2017). Recordings were conducted using a Multiclamp 700B amplifier, Digidata 1440A and pClamp 10.6 software (Molecular Devices). Series resistance was compensated to ~70% and leak was subtracted offline in Clampfit 10 software. Cells with <100 pA negative bias current at a resting potential of −70 mV were accepted in voltage-clamp recordings. Cells were rejected if access resistance exceeded 40 MΩ. Recordings were obtained at room temperature (22–24°C) in a bath solution composed of (mM): 120 NaCl, 3 $NaHCO_3$, 3.5 KCl, 1.5 $MgCl_2$, 1.5 $CaCl_2$, 10 HEPES, 10 D-Glucose, pH 7.4 with NaOH. The bath solution also contained 2 mM 4-AP, 2 mM CsCl, 100 nM apamin and 100 nM paxilline, and the internal electrode solution contained 1 μM TRAM-34 to block a wide spectrum of potassium channels potentially expressed in tsA-201 cells. Despite this a small background presumed potassium current of <200 pA could be detected for a command pulse to 40 mV, but this was not blocked by the Kv7 channel blocker 10 μM XE-991. The internal electrode solution was composed of (mM): 110 $KMeSO_4$, 30 KCl, 10 HEPES, 2 $MgCl_2$, 2 ATP, 0.5 GTP, 5 phosphocreatine, 0.5 EGTA and 0.47 CaCl2. CBD in methanol (Sigma-Aldrich) was stored at −20°C and added acutely to the external solution. To reduce potential binding of CBD to plastic, all perfusion lines and the recording chamber were washed with 70% ethyl alcohol and flushed with distilled water before introducing a new coverslip for recordings during acute applications of CBD.

Biotinylation

Transfected tsA-201 cells were biotinylated by treating with 1.5 mg/mL Sulfo-NHS-SS-biotin (Thermo Fisher, CA#PG82077) before being lysed in a buffer containing (in mM): 150 NaCl, 50 Tris, 2.5 EGTA, 1% NP-40, and proteinase inhibitor (Roche, 04693124001), pH 7.5 (Yao et al., 2020). To enrich biotinylated proteins, 500 μg of total proteins were incubated with streptavidin agarose beads (Thermo Fisher, CA#20359) for 2 h at 4°C. Proteins were eluted and boiled in a 4x sample buffer (Bio-Rad, CA#1610747) before being resolved in SDS-PAGE. Western blotting was conducted using a rabbit anti-Kv7.2 antibody (1:1000, Cell Signaling Tech,14,752), a rabbit anti-Kv7.3 antibody (1:1000, Alomone, APC-051), and a mouse anti-GAPDH antibody (1:1000, Invitrogen, 39–8600). The secondary antibodies used were the HRP conjugated goat anti-mouse IgG antibody (1:3000, Invitrogen, 62–6520) or HRP conjugated donkey anti-rabbit IgG antibodies (1:5000; GE Health, NA9340V). Band density was analyzed with ImagLab (Bio-Rad).

Immunostaining

For dSTORM imaging tsA-201 cells were grown on 18 mm No 1.5 coverslips (Electron Microscopy Sciences, PA, USA) at 37°C. For dual color dSTORM tsA-201 cells were transfected with HA-tagged Kv7.3 cDNA (0.5 μg) and either Kv7.2 wildtype (0.5 μg) or Kv7.2 mutant (0.5 μg). After 36–48 h cells were washed with phosphate-buffered saline (PBS) and fixed in 4% paraformaldehyde (PARA) (Electron Microscopy Sciences, ON) in PBS for 10 min. After 3 washes in PBS cells were incubated with a blocking medium consisting of 3% (v/v) donkey serum and 3% (v/v) goat serum (Jackson ImmunoResearch), 2% (v/v) dimethyl sulfoxide (BDH VWR Analytical) and 0.1% (v/v) Tween 20 (Sigma Aldrich) in PBS for 45 min at RT (~25°C). Cells were sequentially incubated in blocking solution containing the primary antibodies rabbit monoclonal anti-Kv7.2 (1:250; 14,752, Cell Signaling Technology) and then mouse monoclonal anti-HA (1:250; ab130275, Abcam). Primary antibodies were incubated with cells for 45 min at RT with three washes of blocking solution between each incubation. After five 10 min washes in blocking medium at RT cells were sequentially treated with Alexa Fluor 647 conjugated donkey $F(ab')_2$ anti-rabbit IgG (1:1000, 711-606-152, Jackson ImmunoResearch) then Cy-3 conjugated goat $F(ab')_2$ anti-mouse IgG (1:1000, 115-166-146, Jackson ImmunoResearch) for 45 min (RT) with three 5 min washes in blocking solution between secondary antibody incubations. After three rounds of 10 min washes in blocking solution cells were washed once in PBS and post fixed with 4% PARA and 0.1% glutaraldehyde in PBS for 10 min followed by three 10 min washes in PBS. TetraSpek™ beads (1:2000, 100 nm diameter, T7279, Thermofisher) were added to coverslips overnight at 4°C in PBS. Coverslips received three 5 min washes in PBS to remove loose fiducial beads. Labeling and imaging was performed on cells prepared from a minimum of 2 different experiments.

Super-resolution imaging

Direct Stochastic Optical Reconstruction Microscopy (dSTORM) imaging was performed using a Quorum Diskovery Flex microscope equipped for TIRF illumination (150 nm depth) using an HC Plan Apo 63X/NA 1.47 oil immersion objective, and an Andor iXon Ultra 897 EMCCD camera (Sahu et al., 2019). Stronger intensity laser illumination was first used to photoswitch fluorophores into a temporary dark state (laser power: 561 nm, 55 mW @ 100%; 647 nm, 53 mW @ 100%). Subsets of active blinking fluorophores were then imaged at a lower laser intensity (70–95% excitation) at a 33 Hz frame rate. During image acquisition the 405 nm laser line was adjusted to obtain a balanced reactivation of Alexa Fluor 647 or Cy-3 dyes to collect 15,000 to 25,000 image frames per sample to be processed offline.

Image reconstruction was carried out using ThunderSTORM (Fiji, ImageJ) to wavelet filter image streams (Pixel size: 150.5 nm; photoelectrons per A/D count: 8.98; base level A/D count: 200; EM gain: 200) and be rendered as a 2D Gaussian fit to localize centroids (Sahu et al., 2019). In most cases mechanical drift over the time frame required for imaging (20–30 min) ranged no more than 0–500 nm, with any cases approaching 700 nm excluded from analysis. X and Y positional coordinates and intensity information of point localizations were further analyzed using Localization Microscopy Analyzer (LAMA) software (Malkusch and Heilemann, 2016) and MATLAB. The X-Y coordinates of 3–6 100 nm fiducial TetraSpek beads (T7279, Thermofisher) were used as the reference point to align signals using the affine registration function of LAMA. Morphological cluster analysis and nearest neighbor Euclidean distances were conducted in LAMA (Malkusch and Heilemann, 2016) and MATLAB, and overlap of neighboring clusters assessed using an a Manders correlation coefficient and Pearson correlation coefficient (FIJI, JACoP) (Bolte and Cordelières, 2006).

Spectral-FRET imaging

The approaches used to detect Fluorescence Resonance Energy Transfer (FRET) followed that previously reported (Asmara et al., 2017; Sahu et al., 2017; Wallrabe and Periasamy, 2005). Briefly, tsA-201 cells were transiently transfected with proteins tagged with EGFP as the donor or mKate2 as the acceptor fluorophore. Constructs used here included Kv7.2wt-EGFP, Kv7.2mut-EGFP, and Kv7.2wt-mKate2, Kv7.3-mKate2. Fluorescence tagged Kv7 channels were transfected at 0.3 μg/dish, and EGFP and mKate2 alone at 0.1 μg/dish. Before imaging, the cell medium was replaced with low K^+-based imaging medium composed of (mM): 148 NaCl, 1 KCl, 10 HEPES, 3 $CaCl_2$, 10 glucose, 1 $MgCl_2$, pH 7.3 at 25°C. Spectral-FRET was imaged using a Leica SP8 microscope (Leica, Germany) with a 40X NA 0.8 water immersion objective and a 488 nm laser line to excite EGFP and 552 nm to excite mKate2 in confocal images and for mKate2 photobleaching. Spectral images were obtained by exciting cells at 488 nm and emission spectra were recorded between 495 nm and 750 nm. LAS X (Leica) were used to linearly unmix EGFP and mKate2 spectra signals and the intensity of EGFP before and after photobleaching of mKate2 was quantified in ImageJ.

QUANTIFICATION AND STATISTICAL ANALYSES

Activation curves of Kv7 channels were fitted according to the Boltzmann equation: $G/(G - Gmax) = 1/(1 + \exp((Va - V)/k))$, where G is calculated with equation $G = I/(V - Vrev)$, Va is the half activation potential and k is the slope factor. Activation plots were fitted using OriginPro 9.0 (OriginLab, Northampton, MA).

All average values are represented as mean ± S.E.M unless otherwise indicated. Statistical methods used for comparison consist of Student's *t* test, Welch's t-test when variance was significantly unequal, Mann-Whitney test and two-way ANOVA followed by Tukey's pairwise comparison when comparing more than two datasets, and were described in the figure legend. For Figures 1, 2, 4, and 5, statistical analyses were conducted with OriginPro 9 or Graphpad Prism 6 (Graphpad Software). For Figure 3, Histograms were evaluated with shapiro-wilks test for normality, Pearsons second moment skew, Fischer-Pearson coefficient of skewness and median using custom R scripts (Celikoglu and Tirnakli, 2018). Cluster density was determined with Fiji where multiple ROIs from one image were pooled into one data point and analyzed using R(v.3.5.1). Manders' correlation coefficients were calculated using "Just another colocalization plugin" (JACoP (Bolte and Cordelières, 2006)) with default thresholding and Pearson Correlation Coefficients calculated using JACoP and statistically compared using functions in R. For all figures no data was excluded from raw datasets. N number represents the number of cells or the number of biological repeats, as indicated in figure legend. $p < 0.05$ was used as a significant difference.